Supplemental Data

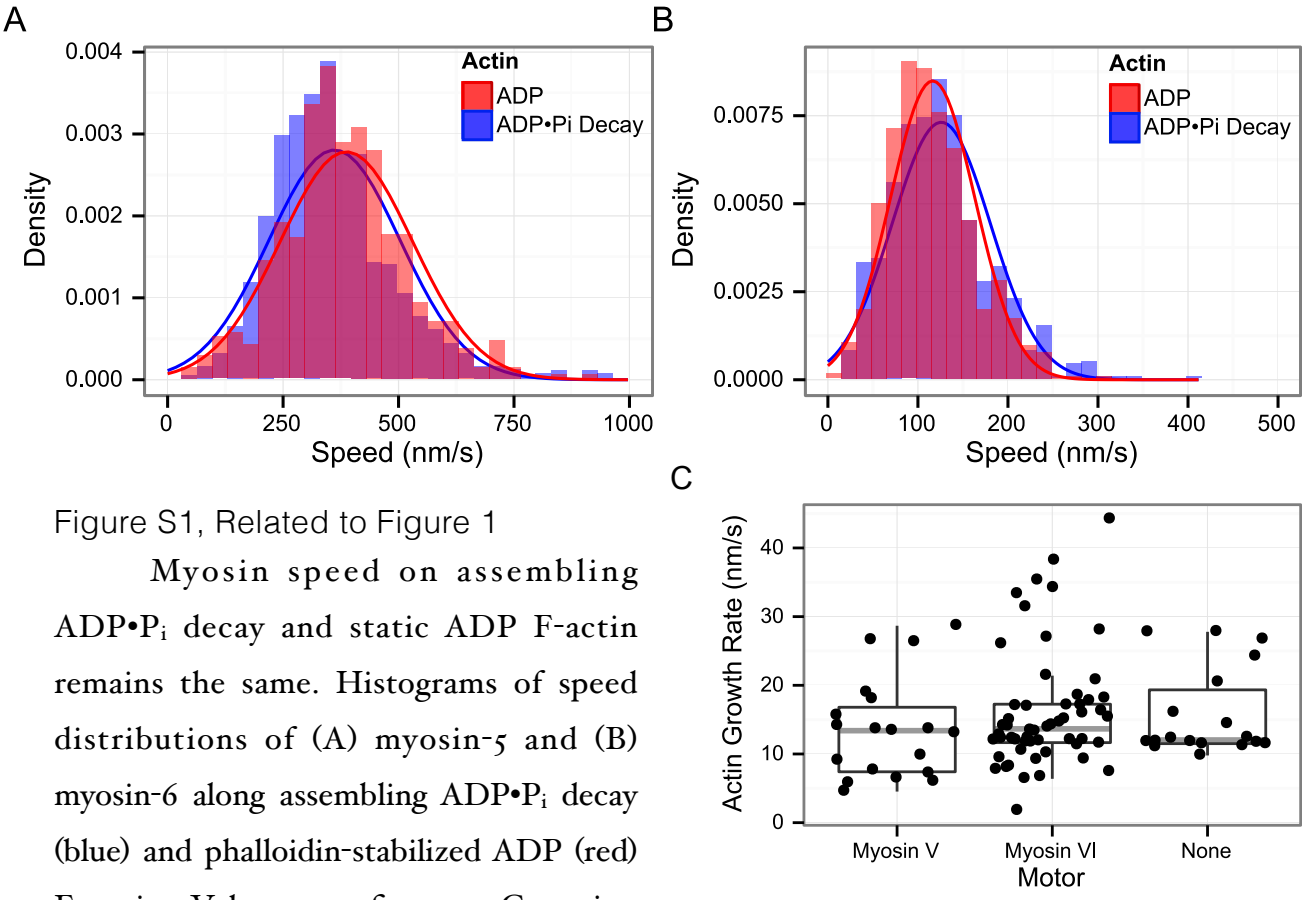

Figure S1, Related to Figure 1

Myosin speed on assembling ADP•P_i decay and static ADP F-actin remains the same. Histograms of speed distributions of (A) myosin-5 and (B) myosin-6 along assembling ADP•P_i decay (blue) and phalloidin-stabilized ADP (red) F-actin. Values are fit to a Gaussian distribution (mean and standard deviations reported in Table S2). Speeds are unaltered for both motors on either F-actin. Speeds are unaltered for either motor under either F-actin condition and correspond to what has been reported previously [S1]. (C) Growth rates of assembling F-actin in the presence of myosin-5 and myosin-6 remain the same. Growth rates of assembling F-actin were determined in the presence and absence of myosin-5 or myosin-6. The average growth rate of assembling F-actin remains unchanged under the influence of myosin-5 or myosin-6.

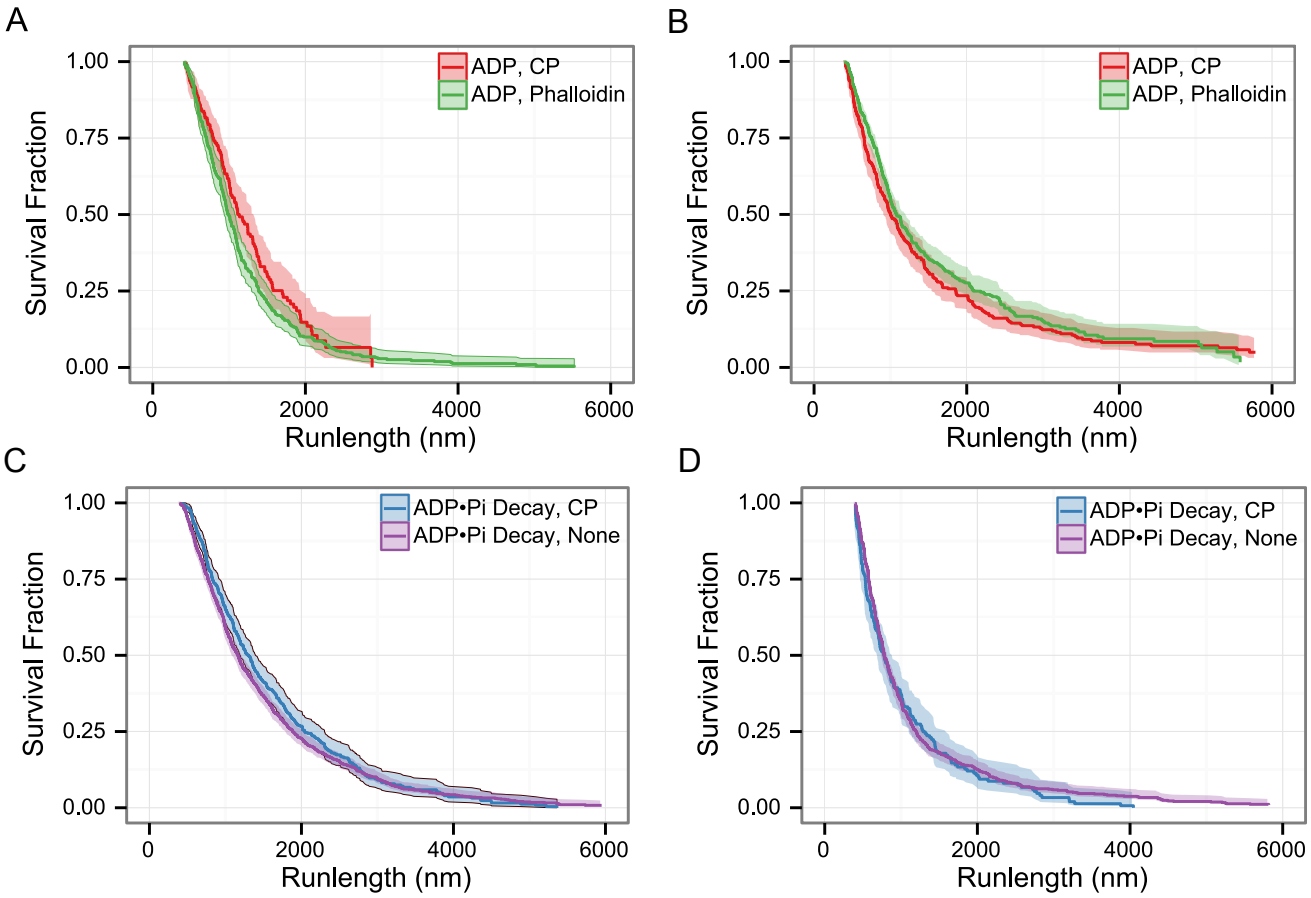

Figure S2, Related to Figure 2

The actin filament stabilizer does not affect myosin runlengths. (A) Runlength measurements of myosin-5 (left) and myosin-6 (right) on F-actin assembled, aged, and stabilized with phalloidin; vs. F-actin assembled to desired filament length, capped with CP and aged. Both conditions yield ADP F-actin. Myosin-5 and myosin-6 take runs of similar length on both types of ADP actin. (B) Runlength measurements of myosin-5 (left) and myosin-6 (right) on F-actin assembled without stabilizer (ADP•P_i Decay, None) or assembled to the desired length and capped with CP (ADP•P_i Decay). Myosin-5 and myosin-6 runlengths are similar on both types of ADP•P_i F-actin. Taken together, these observations rule out either stabilizer as the source of the altered runlengths. The Kaplan-Meier estimate of the run length survivor function is shown. Events are left truncated at 0.4 μm and are right censored at filament ends. Bands indicate the 0.95 CI.

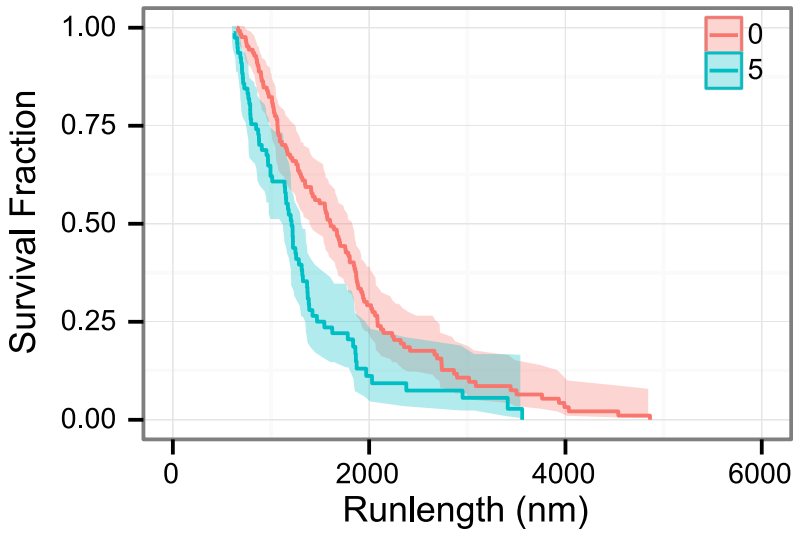

Figure S3, Related to Figure 3

Myosin-5 runlengths change as filaments age on the minute timescale. Filaments were assembled to the desired length (~6 min), capped with CP, and aged for the indicated times in minutes (after CP addition and before imaging with myosin-5). These filament assembly conditions are similar to those in Figure 2D. Imaging was completed within 5 min. Myosin-5 traveled a mean distance of 1200 ± 80 nm (SEM, n = 126) on the 0 min F-actin and 750 ± 80 nm (SEM, n = 78) on the 5 min old F-actin. The runlength distance was statistically significant ($p = 4 \times 10^{-5}$, log-rank test). These runlengths are comparable to those of ADP F-actin and ADP•P_i Decay F-actin from Figure 2B (1200 nm and 790 nm, respectively, Table S1). Thus, F-actin conversion occurs within minutes, consistent with the timescale of P_i release.

Motor	Actin State	Actin Stabilizer	n	Mean Speed (nm/s, ± SD)
myosin-5	**ADP**	**Phalloidin**	315	360 ± 130
myosin-5	**ADP**	**CP**	146	410 ± 180
myosin-5	**ADP·P_i Decay**	**None**	989	370 ± 130
myosin-5	**ADP·P_i Decay**	**CP**	428	350 ± 150
myosin-5	**ADP·P_i**	**Phalloidin-Copoly**	263	420 ± 130
myosin-6	**ADP**	**Phalloidin**	476	120 ± 51
myosin-6	**ADP**	**CP**	279	110 ± 40
myosin-6	**ADP·P_i Decay**	**None**	707	130 ± 56
myosin-6	**ADP·P_i Decay**	**CP**	133	110 ± 44
myosin-6	**ADP·P_i**	**Phalloidin-Copoly**	249	140 ± 54

Table S1, Related to Figure S1

Velocity summary statistics for myosin motors moving along F-actin with the set of nucleotide states and filament stabilizers.

Motor	Actin State	Actin Stabilizer	n	Mean Runlength (nm, ± SEM)	Median Runlength (nm)	0.95 CI (nm)
myosin-5	**ADP**	**Phalloidin**	315	790 ± 40	600	540 - 670
myosin-5	**ADP**	**CP**	146	890 ± 60	740	620 - 910
myosin-5	**ADP·P_i Decay**	**None**	989	1100 ± 40	760	700 - 820
myosin-5	**ADP·P_i Decay**	**CP**	428	1200 ± 50	900	800 - 990
myosin-5	**ADP·P_i**	**Phalloidin-Copoly**	263	1200 ± 60	910	790 - 1100
myosin-6	**ADP**	**Phalloidin**	476	1300 ± 90	680	610 - 800
myosin-6	**ADP**	**CP**	279	1300 ± 120	600	530 - 730
myosin-6	**ADP·P_i Decay**	**None**	707	770 ± 50	380	360 - 430
myosin-6	**ADP·P_i Decay**	**CP**	133	650 ± 60	380	300 - 470
myosin-6	**ADP·P_i**	**Phalloidin-Copoly**	249	360 ± 30	220	170 - 260

Table S2, Related to Figure 2

Runlength summary statistics for myosin motors moving along F-actin with the set of nucleotide states and filament stabilizers.

Motor	Actin P(ADP·P_i)	n	Mean Runlength (nm, ± SEM)	Median Runlength (nm)	0.95 CI (nm)
myosin-5	**0.00 - 0.66**	853	1200 ± 50	800	760 - 910
myosin-5	**0.66 - 1.00**	256	1300 ± 110	990	820 - 1500
myosin-6	**0.00 - 0.33**	405	1200 ± 140	450	380 - 550
myosin-6	**0.33 - 1.00**	397	660 ± 50	390	350 - 450

Table S3, Related to Figure 3

Runlength summary statistics for myosin-5 and myosin-6 moving along assembling actin within bands of different nucleotide states along the filament.

Supplemental Experimental Procedures

Protein expression and purification

Actin was purified from rabbit skeletal-muscle acetone powder (Peel Freez Biologicals) [S2] and labeled on Cys374 with Tetramethylrhodamine-6-maleimide (TMR, Invitrogen-Molecular Probes), or biotin-maleimide (Company?) [S3].

The myosin-5-HMM-GCN4-YFP-Flag construct contains the first 1107 amino acids of chicken myosin-5a, with a leucine zipper (GCN4) fused in frame to the native coiled-coil to ensure dimerization [S4] and YFP fused to its C-terminus. To facilitate purification, a FLAG-tag epitope (GDYKDDDDK) was introduced at the N-terminus. Myosin-5 was expressed using recombinant baculovirus in Sf9 insect cells that were also co-infected with recombinant baculovirus expressing calmodulin and the specific light-chain MLC-1sa from human. The myosin-6-HMM-GCN4-Flag-Ctag contains the first 994 amino acids of porcine myosin-6, with a leucine zipper (GCN4) fused in frame to the native coiled-coil to ensure dimerization, a Flag-tag for purification, and a Ctag for Cy5 fluorescent labeling using separately expressed and labeled Clamp protein [S5]. Myosin-6 was cloned into the InsectDirect vector pBiEx3 (Novagen) and expressed in Sf9 insect cells as previously described [S6, 7]. All myosins were purified via Flag-tag affinity chromatography as previously described [S3, 8] and dialyzed overnight at 4 ˚C against buffer containing 25 mM imidazole, pH 7.5, 50 mM KCl, 4 mM $MgCl_2$, 1 mM EGTA, 10 mM DTT, and 50% glycerol, and stored at -20 ˚C. Affinity clamp protein with a single cysteine residue was expressed, purified and labeled with Cy5 as previously described [S5, 9]. To label myosin-6, Cy5-Clamp protein was used at a 5-fold molar excess over purified Ctag-labeled myosin.

Actin was purified from chicken skeletal muscle and labeled with either TMR-maleimide or biotin-maleimide at Cys 374 as previously described [S10-12]. The G-actin used for assembly at 1 µM concentration contained 5% TMR-labeled actin monomers and 0.1% biotinylated actin monomers.

Mouse capping protein was expressed and purified as described previously [S13], and was stored in buffer containing 10 mM Tris, pH 7.5, 40 mM KCl, 0.5 mM DTT, and 50% (v/v) glycerol.

TIRF microscopy

Microscope cover glasses (24x40 mm, Fisher Scientific) were piranha cleaned and coated with PEG-biotin-silane (3.4k PEG-Biotin-Silane:5k PEG-Silane, 1:1000, Laysan Bio Inc.), and flow chambers (20 x 3 mm) were built as described [S14]. Immediately before each experiment, the glass surface was coated with neutravidin (0.5 mg/mL in water), blocked with bovine serum albumin (5 mg/ml in 2 mM Tris-Cl, pH 8.0, 0.2 mM ATP, 0.5 mM DTT, 1 mM NaN_3, 0.1 mM $CaCl_2$), and rinsed with the same buffer. Imaging experiments were performed in TIRF buffer: 10 mM imidazole pH 7.0, 50 mM KCl, 1 mM $MgCl_2$, 1 mM EGTA, 50 mM DTT, 0.2 mM ATP, 15 mM glucose, 20 µg/mL catalase, 100 µg/mL glucose oxidase, and 0.5% methylcellulose (400 CP). Myosins and actins were added to the flow chamber as indicated below, under "F-actin conditions". TIRF microscopy images of biotinylated TMR-labeled actin (ex: 561 nm), and Myosin-5-YFP (ex: 488 nm) were collected at 0.5 s exposure with an iXon plus X-4818 EMCCD camera (Andor Technology) using an Olympus IX-50 microscope equipped with a plan-apochromatic through-the-objective TIRFM illumination lens (100 x, N.A. 1.45). The Cy5-labeled myosin-6 construct was imaged using a home-built inverted TIRF microscope likewise equipped with an Olympus super-apochromatic objective (100 x, N.A. 1.40) attached to an iXon charge-coupled device (model No. DV887ECS-BV; Andor Technology) at 0.5 s exposure. Actin and myosin imaging were performed simultaneously using a dual-view arrangement to project the two color channels on separate halves of the camera.

Qualitatively, in the assembling actin assays we note a reduced incidence of "dead" myosins that adhere to the coverslip away from long filaments, with an overall improvement in imaging quality. This observation suggests that many of these dead myosins actually bind to unresolved, short segments of actin under the standard phalloidin-stabilized filament condition.

F-actin conditions

For all of the following conditions a final actin concentration of 1 µM Mg-ATP-actin was prepared by mixing stocks of Mg-ATP-actin (5% TMR-actin, 0.1% Biotin-actin, in G-buffer: 2 mM Tris-Cl, pH 8.0, 0.2 mM ATP, 0.5 mM DTT, 1 mM NaN3) into polymerization TIRF buffer. Myosin was added at 1-5 µM. Unless mentioned otherwise, capping protein

was added at 10 nM and phalloidin (Sigma, dissolved in methanol) at 1 µM final concentrations.

ADP•P_i Decay Assembling F-actin (Figure 2A, iii; Figure 2BC)

TIRF buffer containing Mg-ATP-actin and fluorescently labeled myosin was applied to the flow cell, followed by imaging.

ADP Phalloidin-stabilized F-actin (Figure 2A, i; Figure 2BC)

20 to 25 hours prior imaging, Mg-ATP-actin was polymerized at RT for 60 min, stabilized by adding 1 µM phalloidin, and stored on ice. Imaging chambers were prepared by perfusing actin filaments in TIRF buffer, incubating for 6-8 min, adding fluorescently labeled myosin, followed by imaging.

ADP•P_i Decay CP F-actin (Figure 2A, iv; Figure 2DE)

Mg-ATP-actin was polymerized in the imaging chamber for ~6-8 min. Capping protein (10 nM) was perfused into the imaging chamber to terminate filament assembly along with fluorescent myosin, followed by imaging.

ADP CP F-actin (Figure 2A, ii; Figure 2DE)

20 to 25 hours prior imaging, Mg-ATP-actin was polymerized in the dark at RT for 60 m in an Eppendorf tube. Polymerization was terminated by adding 10 nM capping protein. The mix was stored on ice until imaging. The actin was perfused into the imaging chamber and allowed to attach for 6-8 min. Fluorescently labeled myosin was added to the flow cell, followed by imaging. This condition does not contain phalloidin.

ADP•P_i Phalloidin-Copolymerized F-actin (Figure 2A, v; Figure 2FG)

Mg-ATP-actin and 1 µM phalloidin was mixed simultaneously in TIRF buffer to initiate polymerization, perfused into the imaging chamber, and incubated in the dark at RT for 15 min to produce 20-30 µm long actin filaments. Filament assembly was stopped by adding 10 nM capping protein and 1 µM phalloidin in TIRF buffer to prevent filaments from disassembling and to further stabilize the F-actin. The flow cell was stored in the dark under high humidity at 4˚C until imaging. After 1-20 hours, TIRF buffer containing

fluorescently labeled myosin, 10 nM capping protein and 1 μM phalloidin was perfused into the imaging chamber, followed by imaging.

F-actin for time-course (Figure S4)

Mg-ATP-actin was polymerized in the imaging chamber for ~6-8 min. Capping protein (10 nM) was perfused into the imaging chamber to terminate filament assembly, followed by imaging at the indicated times. For t = 0 min, fluorescently labeled myosin was included in capping protein-containing TIRF buffer and imaging was performed immediately. For t = 5 min, fluorescently labeled myosin was added 5 min after filament assembly had been stopped by capping protein, and imaging was performed immediately. Motility data from approximately the first 5 min of each condition were analyzed.

Data analysis and quantification

Motor runs and filament ends were traced manually using ImageJ, and trajectory runlengths, velocities, landing events and actin ages along the trajectories were extracted using custom scripts written in Julia [S15]. The R package "survival" was used for runlength analysis. We traced each analyzed actin filament, and projected the movie data along the tracing and along the time axis to generate a kymograph. We used the final frame of the movie to trace growing filaments. Kymographs of the growing filaments show both the growth of the filament at the barbed end, as well as the movement of myosins along the filament. To correlate myosin properties with actin nucleotide state as in Figure 3, we record the elapsed time, t, since the actin monomer first appeared at each position in a recorded myosin run. In cases where a segment of the filament was present at the start of the movie, the observed barbed end growth was linearly projected back to zero length to determine the monomer appearance time within the unobserved segment. As actin monomers age after addition to the barbed end, they decay to the ADP•P_i state with a rate constant k = 0.0026 s^{-1} [S16]. We thus calculate the probability of the actin ADP•P_i state, P(ADP•P_i), for each observed position in a motor run, as P = exp(-kt). We show these probabilities on the example kymograph in Figure 3A.

All runlength plots are shown as Kaplan-Meier estimators of the survival curves [S17]. Using the Kaplan-Meier estimator allows us to properly account for common situations that would cause us to underestimate true runlengths, because we can handle

information from right-censored events. In contrast, the most common runlength analysis method in the field is construction of a PDF (histogram) directly from the runlength data, which does not allow for proper correction of these right-censored events. Right-censoring occurs when we underestimate the true runlength of an event. This underestimation occurs when a myosin runs off of the actin filament end, runs that start or end on the first or last frame of the movie, and runs that cross the threshold P(ADP•P_i) values shown in Figure 3. For the threshold-crossing runs in Figure 3, we split the runs into two smaller runs at the threshold. Both of these two runs are then treated as right-censored in their corresponding category. This treatment is similar in concept to "masking" the kymograph for each P(ADP•P_i) band, and considering how runs obtained from the two masked regions would be censored.

Supplemental References

S1 Ali, M. Y., Previs, S. B., Trybus, K. M., Sweeney, H. L., and Warshaw, D. M. (2013). Myosin VI has a one track mind versus myosin Va when moving on actin bundles or at an intersection. Traffic, *14*, 70-81.

S2 Spudich, J. A. and Watt, S. (1971). The regulation of rabbit skeletal muscle contraction. I. Biochemical studies of the interaction of the tropomyosin-troponin complex with actin and the proteolytic fragments of myosin. J Biol Chem, *246*, 4866-71.

S3 Rock, R. S., Rice, S. E., Wells, A. L., Purcell, T. J., Spudich, J. A., and Sweeney, H. L. (2001). Myosin VI is a processive motor with a large step size. Proc Natl Acad Sci U S A, *98*, 13655-9.

S4 Trybus, K. M., Freyzon, Y., Faust, L. Z., and Sweeney, H. L. (1997). Spare the rod, spoil the regulation: necessity for a myosin rod. Proc Natl Acad Sci U S A, *94*, 48-52.

S5 Huang, J., Nagy, S. S., Koide, A., Rock, R. S., and Koide, S. (2009). A peptide tag system for facile purification and single-molecule immobilization. Biochemistry, *48*, 11834-6.

S6 Nagy, S. and Rock, R. S. (2010). Structured post-IQ domain governs selectivity of myosin X for fascin-actin bundles. J Biol Chem, *285*, 26608-17.

S7 Ricca, B. L. and Rock, R. S. (2010). The stepping pattern of myosin X is adapted for processive motility on bundled actin. Biophys J, *99*, 1818-26.

S8 Nagy, S., Ricca, B. L., Norstrom, M. F., Courson, D. S., Brawley, C. M., Smithback, P. A., and Rock, R. S. (2008). A myosin motor that selects bundled actin for motility. Proc Natl Acad Sci U S A, *105*, 9616-20.

S9 Huang, J., Koide, A., Makabe, K., and Koide, S. (2008). Design of protein function leaps by directed domain interface evolution. Proc Natl Acad Sci U S A, *105*, 6578-83.

S10 Pardee, J. D. and Spudich, J. A. (1982). Purification of muscle actin. Methods Cell Biol, *24*, 271-89.

S11 Kudryashov, D. S. and Reisler, E. (2003). Solution properties of tetramethylrhodamine-modified G-actin. Biophys J, *85*, 2466-75.

S12 Rock, R. S., Rief, M., Mehta, A. D., and Spudich, J. A. (2000). In vitro assays of processive myosin motors. Methods, *22*, 373-81.

S13 Falck, S., Paavilainen, V. O., Wear, M. A., Grossmann, J. G., Cooper, J. A., and Lappalainen, P. (2004). Biological role and structural mechanism of twinfilin-capping protein interaction. EMBO J, *23*, 3010-9.

S14 Winkelman, J. D., Bilancia, C. G., Peifer, M., and Kovar, D. R. (2014). Ena/VASP Enabled is a highly processive actin polymerase tailored to self-assemble parallel-bundled F-actin networks with Fascin. Proc Natl Acad Sci U S A, *111*, 4121-6.

S15 Bezanson, J., Edelman, A., Karpinski, S., and Shah, V. (2014). Julia: A fresh approach to numerical computing. http://arxiv.org/abs/1411.1607

S16 Melki, R., Fievez, S., and Carlier, M. F. (1996). Continuous monitoring of Pi release following nucleotide hydrolysis in actin or tubulin assembly using 2-amino-6-mercapto-7-methylpurine ribonucleoside and purine-nucleoside phosphorylase as an enzyme-linked assay. Biochemistry, *35*, 12038-45.

S17 Kaplan, E. L. and Meier, P. (1958). Nonparametric estimation from incomplete observations. Journal of the American Statistical Association, *53*, 457–481.